

# Role of lunar laser ranging in realization of terrestrial, lunar, and ephemeris reference frames

Dmitry Pavlov

Received: date / Accepted: date

**Abstract** Three possible applications of lunar laser ranging to space geodesy are studied. First, the determination of daily Earth orientation parameters (UT0 and variation of latitude), which is rarely used nowadays in presence of all-year VLBI, SLR, and GNSS data. The second application is the determination of two (out of three) lunar orientation parameters, i.e. daily corrections to the rotational ephemeris of the Moon. It may be of importance for the future lunar satellite-based navigational systems. The third application is the tie of ephemeris frame (BCRF) to the ICRF. It has been studied before, though in this work it is extensively compared to another realization of the same tie, obtained by spacecraft VLBI observations; also, two different EOP series and two different models of tidal variations of geopotential are applied, with different outcomes on the tie.

The EPM lunar-planetary ephemeris, along with its underlying dynamical model and software, was used to obtain the presented results. All available observations were processed, since the earliest made at the end of 1969 at the McDonald observatory till the end of July 2019 (Matera, Grasse and also Wettzell observatory which began to provide data in 2018). The results and some open questions are discussed.

## 1 Introduction

Lunar laser ranging (LLR), being the most precise technique of observation of the relative motion of two Solar system bodies, through 50 years of existence

---

D. Pavlov  
Institute of Applied Astronomy of the Russian Academy of Sciences (IAA RAS)  
Russia, 191187, St. Petersburg, Kutuzova Embankment, 10  
Tel.: +7 (812) 275-1118  
Fax.: +7 (812) 275-1119  
E-mail: dpavlov@iaaras.ru

has produced many scientific results. Some of them are dedicated to fundamental properties of spacetime (see e.g. [25, 78, 79, 70, 24])<sup>1</sup>, while some others have provided new information about tides on the Earth [76], and tides and the internal structure of the Moon [75, 41, 51]. In addition to the theoretical results, LLR has allowed to build a high-precision geocentric ephemeris of the Moon, featuring both orbital and rotational motion [17, 58, 70]. The building of such ephemeris is usually accompanied by determination of the positions of lunar laser ranging stations (and velocities for some of them), and the positions of the five lunar retroreflectors. The lunar ephemeris and the positions of the lunar retroreflectors thus form a most precise lunar reference frame that can be used for navigation and orbit determination in future lunar missions, as well as for improvement of currently achieved theoretical results. Russian planned lunar lander Luna-25 will have a retroreflector panel [68] on it; there are also proposals for placing next-generation single corner cubes on the surface of the Moon [10, 61, 67, 2].

There are just a few LLR stations in the world. They operate independently from each other and are constrained by light and weather conditions and Moon's visibility. Hence, the events of LLR from different stations on the same day are rare. Still, with one station operating on one day, it is possible to determine two daily (nightly) corrections to Earth rotation angles: UT0 and VOL (variation of latitude), which are mathematically the same as daily corrections to the station's longitude and latitude, respectively. These corrections brought a significant contribution to the determination of the terrestrial pole and Universal time in 1970–1980s, see e.g. [35, 12] or [8, pp. M-17–M-20], and are still calculated and used in JPL KEOF EOP series [62].

Known EOP series that combine terrestrial and celestial poles—namely, IERS C04 [4] and IERS Bulletin A [11, pp. 94–116]<sup>2</sup> are constructed without using LLR data. However, the Moon has a much more stable orbit than the artificial satellites used in SLR and GNSS observations. One reason for that is the Moon experiencing smaller perturbations from nonspherical gravitational potential of the Earth than do artificial satellites at low orbits; another reason is that the solar pressure acceleration of the Moon is very small and almost non-intermitting. Also, unlike GNSS and VLBI, LLR observations do not suffer from daily clock offsets. That, together with increasing precision and frequency of LLR observations worldwide, suggests that the LLR might be helpful in the future for EOP determination.

It is well known that the LLR observations are sensitive not only to the Earth's equator plane, but also to Earth's orbit plane, due to the Sun affecting the orbit of the Moon (see e.g. [74]). That makes LLR different from radio ranging observations of e.g. Mars orbiters which have an accuracy of 55 cm at best [32]. Laser ranging to the distance of Mars or Venus has not ever been

---

<sup>1</sup> A collection of materials on LLR and relativity is available at <http://www.issibern.ch/teams/lunarlaser>

<sup>2</sup> Another EOP series that provides both terrestrial and celestial poles is JPL EOP2: <https://eop2-external.jpl.nasa.gov>. This relatively new product was unknown to author at the time of writing.

done. The accuracy of 55 cm means sub- $\mu$ as sensitivity to the ecliptic plane at the distance of orbit of Mars, but mere 18 mas sensitivity to Earth orientation at best. On the other hand, VLBI observations of quasars, widely used to determine the orientation of the Earth's equator w.r.t. celestial frame, have quite low sensitivity to the orbit of the Earth.

The sensitivity of LLR to both ecliptic and equator, among other things, allowed to determine the value of obliquity of the ecliptic  $\epsilon_{J2000} = 84381.406''$  in [7], which is still included to this day into the IAU system of astronomical constants [36].

There have been attempts to determine the celestial pole, in the form of corrections to nutation theory, via LLR [73,82,3,23]. The results are not as accurate as the ones obtained by VLBI. Moreover, there are two major problems with determining the celestial pole by LLR:

1. The constant corrections to celestial pole orientation, while can be formally determined from the LLR, are not separable from the orientation of the Sun–Earth–Moon system, or the whole ephemeris frame, in the celestial frame. If the ephemeris (especially Earth orbit around the Sun) is fixed in the analysis, it constrains the determined orbit of the Moon to have a certain orientation in the celestial frame.
2. Linear or periodic terms in celestial pole, while can be formally determined from LLR, are hard to separate from similar terms coming from the imperfection of the model of the lunar motion, specifically from Earth tides, lunar tides, or lunar core.

A straightforward solution to both problems is to avoid processing LLR observations alone, but always process them together with an EOP series that include the celestial pole determined from VLBI observations. Thus the doubts about the celestial pole should be eliminated and we will be able to treat the found “corrections to celestial pole” as corrections to ephemeris frame orientation (for constant terms, item 1 above), or to the lunar theory (for linear or periodic terms, item 2 above). In reality, however, things become more difficult, which will be shown in Section 7.

## 2 Data

### 2.1 LLR observations

All available LLR observations from late 1960 up to the end of July, 2019 were used in the experiments. Table 1 shows the number and timespan of observations processed from each station.

Apache Point Observatory observations [46,45] were downloaded from the APOLLO website<sup>3</sup>. Observations for McDonald/MLRS1/MLRS2 [64], Haleakala [5], and Grasse (Ruby and YAG [63] lasers) were downloaded from the Lunar Analysis Center of Paris Observatory (POLAC<sup>4</sup>). Green and infrared [9] Grasse

<sup>3</sup> [http://physics.ucsd.edu/~tmurphy/apollo/norm\\_pts.html](http://physics.ucsd.edu/~tmurphy/apollo/norm_pts.html)

<sup>4</sup> <http://polac.obspm.fr/llrdatae.html>

**Table 1** Lunar laser ranging observations.

Station	Timespan	# of normal points
McDonald, TX, USA	1969–1985	3604
Nauchny, Crimea, USSR	1982–1984	25
MLRS1, TX, USA	1983–1988	631
MLRS2, TX, USA	1988–2013	3653
Haleakala, HI, USA	1984–1990	770
Grasse, France (Ruby laser)	1984–1986	1188
Grasse, France (YAG laser)	1987–2005	8324
Grasse, France (MeO green laser)	2009–2019	1930
Grasse, France (infrared laser)	2015–2019	4762
Matera, Italy	2003–2019	233
Apache Point, NM, USA	2006–2016	2648
Wettzell, Germany	2018–2019	42
<b>Total</b>	<b>1969–2019</b>	<b>27810</b>

observations 2009–2018 were downloaded from Geoazur website<sup>5</sup>; they also appeared on the POLAC website some time later. Grasse observations from 2019 were kindly provided by Jean-Marie Torre. Matera Laser Ranging Observatory observations up to 2015 were downloaded from POLAC, while newer ones, since 2017 were obtained from CDDIS<sup>6</sup>, as well as the Wettzell observations [27]. The Crimean observations were recently found on a shelf [80]. Normal points were made from them by James Williams and Dale Boggs [72]. Both raw observations and normal points are publicly available<sup>7</sup>. They do not have a notable impact on the results and were included for the sake of history.

Each normal point contains a time of firing (UTC), signal delay due to range in UTC seconds, and uncertainty. Some of the given uncertainties were re-weighted before processing. In particular, the uncertainties for selected Matera observations in 2010–2012, with given values below 1 picosecond, were treated as a result of a human error in decimal exponent and scaled 1000x. Uncertainties of Apache Point observations made in 2006–2012 were scaled 2x–6x, as recommended on the APOLLO website. Given uncertainties for Grasse observations since September 1999 have not been normalized to  $1/\sqrt{N-1}$ , where  $N$  is the number of returned photons forming the normal point; the normalization was applied before processing.

Selected groups of older (pre-2000) observations were scaled up 1.2x–1.9x to match the postfit weighted root-mean-square (wrms). See [51] for details.

## 2.2 Planetary observations

VLBI observations of a spacecraft orbiting a planet when it passes near a known radio source are essential for determining a tie between ephemeris frame and ICRF (see Sec. 7). They are also known as  $\Delta$ DOR observations. The

<sup>5</sup> <http://www.geoazur.fr/astrogeo/?href=observations>

<sup>6</sup> [ftp://cddis.gsfc.nasa.gov/pub/slr/data/npt\\_crd](ftp://cddis.gsfc.nasa.gov/pub/slr/data/npt_crd)

<sup>7</sup> <http://iaaras.ru/en/dept/ephemeris/observations>

result of a session of such observations is the angular position of planet w.r.t. the ICRF, either as a one-dimensional projection (in case of single-baseline observations), or two-dimensional astrometrical position (in case of a multiple-baseline observations on Very Long Baseline Array, VLBA). Almost all the data were taken from the webpage of Solar system dynamics (SSD) group at NASA JPL<sup>8</sup>, including single-baseline data obtained from Phobos-2 [22], Magellan, Galileo, Venus Express [18], Mars Reconnaissance Orbiter (MRO), and Mars Odyssey; and also astrometric positions of Saturn obtained from Cassini (in [28] there are three more observations not present at the website). Astrometric positions of Mars obtained from MRO and Odyssey observations on VLBA were taken from [48].

Orbits of the planets are best determined (in the ephemeris frame) from ranging data or spacecraft orbiting Mercury, Venus, Mars, Jupiter, and Saturn, and also from ranging and differenced range observations of Mars landers. Also, older planetary ranging data were used for Mercury and Venus. Optical observations of natural satellites of Jupiter and Saturn from different observatories were used to help determine their planets' orbits.

Most of the data was taken from the aforementioned SSD webpage, including ranging data obtained from MESSENGER [49] and Juno; ranging data obtained from Mars Global Surveyor, Mars Odyssey, and MRO [29]; ranging and differenced range data obtained from Viking [81] and Pathfinder [21], and older radar and optical observation data. Mars Express and Venus Express ranges [44] were downloaded from the Geoazur website<sup>9</sup>. Radar ranging data from Crimea is available on the IAA RAS website<sup>10</sup>.

Processing of planetary ephemeris data, apart from VLBI, is not a topic of this work; we refer the reader to other papers devoted to planetary ephemeris [17, 56, 59].

### 2.3 Earth orientation parameters

IERS C04 EOP series was used for processing of planetary observations. For the processing of LLR observations, both C04 and IERS Bulletin A weekly ("finals.all") were used. While there are similarities between those series, they do not generally agree below 1 mas for a number of reasons:

- C04 is a "long-term" series and contains only past data with the lag of up to one month, while Bulletin A is "rapid" series, containing data up to present and a prediction. Also, Bulletin A is routinely retroactively updated upon the availability of new data. This is not the case with C04, except when it is done after a special decision<sup>11</sup>.

---

<sup>8</sup> [https://ssd.jpl.nasa.gov/?eph\\_data](https://ssd.jpl.nasa.gov/?eph_data)

<sup>9</sup> <http://www.geoazur.fr/astrogeo/?href=observations/base>

<sup>10</sup> <http://iaaras.ru/en/dept/ephemeris/observations>

<sup>11</sup> <ftp://hpiers.obspm.fr/iers/eop/eopc04/updateC04.txt>

- C04 and Bulletin A are produced by different groups with different software, and, while underlying models are the same in general, there can be subtle differences in implementation.
- Both series are calculated from a combination of VLBI, GNSS, and SLR data; details of the combination process differ between the two series [4, 11].

The data were downloaded from the IERS website<sup>12</sup>.

### 3 Software

ERA (Ephemeris Research in Astronomy), version 8 was used for processing the planetary and lunar observations, refining the parameters and integrating the dynamical equations [50]. ERA is based on the Racket programming platform [16, 13] and has SQLite<sup>13</sup> as the database engine.

SOFA library<sup>14</sup> [26] was used for conversion between terrestrial and celestial coordinates and conversion between various time scales.

For numerical integration, an implementation of Adams–Bashforth–Moulton method, modified to handle delay differential equations [1], was used. Time-delayed terms appears in the differential equations of lunar rotation due to the nature of the tidal dissipation.

### 4 Models

#### 4.1 Dynamical model

A single dynamical model of the Solar system (including Moon, planets, asteroids, and Trans-Neptunian objects, TNOs), which serves as the basis for EPM planetary-lunar ephemeris, was used in this work. The planetary part of the model comprises relativistic accelerations of point-masses of the Sun, planets, the Moon, asteroids and TNOs, as well as additional accelerations from solar oblateness and Lense-Thirring effect. The orbital motion of the Earth is also affected by “point mass–figure” accelerations that come from Sun, the Moon, Venus, Mars, and Jupiter. The lunar part of the model comprises similar “point mass–figure” accelerations, as well as torques, and a degree-2 “figure-figure” torque between Earth and Moon. The tidal variations of the gravitational potential of the Earth are taken into account, as far as the orbital motion of the Moon is concerned [76]. Both orbital and rotational motion of the Moon are affected by the rotational and tidal dissipation modeled as variations of the lunar gravitational field and inertia tensor. For more detailed description, we refer to [51] and [56, 60] for the lunar and planetary parts, respectively.

<sup>12</sup> <https://www.iers.org/IERS/EN/DataProducts/EarthOrientationData/eop.html>

<sup>13</sup> <http://sqlite.org>

<sup>14</sup> <http://www.iausofa.org>

One piece of lunar dynamical model particularly important for this work is the model of tidal variations of Earth’s gravitational potential that come from the Moon and the Sun raising periodical ocean and solid tides on the Earth. The orbit of the Moon is perturbed by those variations. There are actually two models that are used interchangeably; they were compared in [51]:

- IERS2010 geopotential variations model [52] with fixed coefficients and amplitudes. Only corrections up to order and degree 2 are taken into account.
- DE430 model [76,17] of direct perturbing acceleration of the Moon. It comes with five time delays for three frequencies and three fixed Love numbers for those frequencies. Of the five time delays, three are fixed “orbital” delays applied when the positions of the perturbing objects (Sun and Moon) are calculated; two rotational delays (for diurnal and semi-diurnal frequencies) are determined parameters.

## 4.2 Reductions

Usual routines were applied during the processing of astronomical observations. IAU2000/2006 precession-nutation model [71] together with IERS EOP series [4] was used for transformation between terrestrial and celestial reference frames. Relativistic delay of signal was calculated according to theoretical approximation [31]; delays from the Sun, Earth, the Moon, Jupiter, and Saturn were added up. Calculation of tropospheric delay of laser signal was performed according to empirical models: zenith delay [42] and mapping function [43]. As for radio observations, the tropospheric delay was already subtracted from the provided data. Displacements of reference points due to solid Earth tides and pole tides were calculated according to the IERS Conventions 2010 [52]. Ocean loading was calculated from HARPOS files obtained from the International Mass Loading Service<sup>15</sup> [53]. Atmospheric loading was not applied.

## 4.3 Lunar orientation parameters

In [51], the following lunar-to-celestial transformation matrix is formulated:

$$R_{L2C} = R_z(\phi)R_x(\theta)R_z(\psi + \Lambda), \quad (1)$$

where  $\phi$ ,  $\theta$ , and  $\psi$  are Euler angles and are part of the state of the dynamical system (see Sec. 4.1), while  $\Lambda$  is a sum of three small kinematic periodic terms unaccounted for in the dynamical model.

We treat  $R_z(\phi)R_x(\theta)$  part in eq. 1 as the lunar celestial pole, and  $R_z(\psi + \Lambda)$  as the lunar counterpart of the Earth rotation angle. Also, we assume that the Moon, like the Earth, experiences stochastic variations in its rotation and in the position of instantaneous axis of rotation in the lunar mantle (lunar pole):

<sup>15</sup> <http://massloading.net>

$$R_{L2C}^* = R_z(\phi)R_x(\theta)R_z(\psi + \Lambda)R_z(-r')R_y(q')R_x(p') \quad (2)$$

We call  $p'$ ,  $q'$ , and  $r'$  the lunar orientation parameters (LOP).  $p'$  and  $q'$  define the position of the lunar pole, while  $r'$  is similar to Earth's (UT1–UTC) correction.

While it is theoretically possible to further extend (2) with the corrections to the lunar celestial pole, there will not be a practical utility in it before the development of astronomical instruments that are sensitive to the position of the lunar celestial pole. There are propositions for such instruments, e.g. lunar polar optical telescope [54] or lunar VLBI station [34]. Even after they are developed, it may happen that the present dynamical model already provides good enough lunar celestial pole and that the corrections are not needed. Presently, with only LLR data available, we restrict LOP to just  $p'$ ,  $q'$ , and  $r'$ .

#### 4.4 Celestial pole

In ephemeris–ICRF tie determination (Sec. 7), the model of ITRS-to-GCRS is the IAU2000/2006 precession-nutation model which is extended with two additional rotations:

$$\begin{aligned} R_{T2C}(t) &= R_x(\Delta X)R_y(\Delta Y)Q(t)R(t)W(t) \\ \Delta X &= \Delta X_0 + \dot{X}(t - t_0) + C_X^\Omega \cos \Omega + S_X^\Omega \sin \Omega \\ \Delta Y &= \Delta Y_0 + \dot{Y}(t - t_0) + C_Y^\Omega \cos \Omega + S_Y^\Omega \sin \Omega \end{aligned} \quad (3)$$

where:

- $W(t)$  is the polar motion matrix, obtained from terrestrial pole from EOP series and adjusted for diurnal and semi-diurnal variations due to zonal and ocean tides;
- $R(t)$  is the Earth rotation matrix, obtained from UT1 from EOP series and adjusted for diurnal and semi-diurnal variations due to zonal and ocean tides;
- $Q(t)$  is the celestial pole matrix, adjusted by  $dX$  and  $dY$  corrections from EOP series;
- $t_0$  is the epoch J2000;
- $\Omega$  is the moon ascending node, precessing with a period of approximately 18.6 years;
- $\Delta X$  and  $\Delta Y$  are determined constant rotations of current ephemeris frame to the ICRF;
- $\dot{X}$  and  $\dot{Y}$  are determined rotational trends of the current ephemeris frame w.r.t. the ICRF;
- $C_X^\Omega$ ,  $S_X^\Omega$ ,  $C_Y^\Omega$  and  $S_Y^\Omega$  are additionally determined artifacts that can appear as a 18.6 year periodic motion of celestial pole w.r.t the ICRF.

$\dot{X}$ ,  $\dot{Y}$ ,  $C_X^\Omega$ ,  $S_X^\Omega$ ,  $C_Y^\Omega$  and  $S_Y^\Omega$  are supposed to be zero because both the ICRF frame, as realized by eq. 3, and the ephemeris frame are assumed to be inertial. However, there are difficulties with those assumptions, see Sec. 7.

## 5 Main solution

A large set of parameters of lunar and planetary models was fitted to data (see Sec. 2) using the nonlinear weighted least-squares method. Lunar and planetary parameters were fit (determined) one after another in several iterations until both solutions converged with a joint lunar-planetary ephemeris, which then served as a basis for the results presented in further sections.

### 5.1 Lunar part

The following parameters were fitted in the lunar solution:

- Geocentric position and velocity of the Moon at epoch;
- Euler angles of lunar physical libration ( $\phi$ ,  $\theta$ ,  $\psi$ ) and their derivatives at epoch;
- Angular velocity of the lunar liquid core at epoch;
- Gravitational parameter of the Earth–Moon system;
- Ratios of undistorted lunar moments of inertia:  $\beta = (C - A)/B$  and  $\gamma = (B - A)/C$
- Stokes coefficients of undistorted lunar gravitational potential:  $C_{32}$ ,  $S_{32}$ , and  $S_{33}$ ;
- Lunar Love number  $h_2$ ;
- Lunar core flattening coefficient;
- Lunar tidal delay;
- Rotational delays  $\tau_{1R}$  and  $\tau_{2R}$  of Earth diurnal and semi-diurnal tides (only if DE430 model of tidal variations of geopotential is used; otherwise, fixed IERS formula is applied);
- Amplitudes of  $l'$  (365 d),  $2l - 2D$  (206 d) and  $2F - 2l$  (1095 d) kinematic terms;
- Selenocentric coordinates of five retroreflectors;
- Terrestrial coordinates of all LLR stations;
- Velocities of McDonald/MLRS1/MLRS2 and Grasse stations<sup>16</sup>;
- 24 biases for chosen stations at chosen periods of time.

A more detailed description of the lunar parameters can be found in [51].

The weighted root-mean-square postfit residuals of LLR observations are given in Table 2. Some observations with unreasonably large residuals were considered erroneous and were rejected from the solution. It is visible that the DE430 tidal model gives better results than IERS2010 (partially thanks to two

<sup>16</sup> for other stations, due to a relatively short timespan of their LLR observations, the velocities were taken from GNSS solutions. See [51] for details.

adjustable parameters); that has already been noticed in [51]. IERS2010 does not have the accuracy needed to model the orbit of the Moon at the centimeter level on time intervals exceeding 20 years; without adjustable parameters, the solution distorts the lunar dissipation model to soak up the acceleration.

The other consequence from 2 is that the “finals” IERS EOP series give systematically better fits than the C04 series; that is unexpected, given that the LLR data was not used in production of either series.

**Table 2** Post-fit statistics of lunar solution. WRMS is one-way and given in cm. Note: for pre-1980 McDonald data, KEOF EOP series was used instead of C04 or “finals”.

Station	Timespan	Used	Rej.	WRMS			
				DE430 tides		IERS2010 tides	
				C04	finals	C04	finals
McDonald	1969–1985	3552	52	20.2	20.1	21.1	20.9
MLRS1	1983–1988	588	43	11.5	11.0	12.4	11.5
MLRS2	1988–2013	3224	429	3.7	3.4	4.3	4.1
Nauchny	1982–1984	25	0	11.1	11.1	11.2	11.2
Haleakala	1984–1990	751	19	6.6	5.8	7.0	6.0
Grasse (Ruby)	1984–1986	1109	79	17.7	16.9	18.5	17.7
Grasse (YAG)	1987–2005	8273	51	1.7	1.5	2.0	1.9
Matera	2003–2019	219	14	3.2	3.1	3.2	3.2
Apache	2006–2016	2632	16	1.50	1.50	1.77	1.78
Grasse (MeO green)	2009–2019	1930	0	1.61	1.64	2.01	1.97
Grasse (infrared)	2015–2019	4761	1	1.30	1.25	1.45	1.40
Wetzell	2018–2019	42	0	1.06	1.08	1.27	1.37

The selenocentric coordinate system, in which the coordinates of five retroreflector panels are determined, is based on the principal axes (PA) of the Moon’s figure. Table 3 lists the positions of the five retroreflectors and their formal errors for the best solution of the four (“finals” EOP and DE430 tidal model). These five points realise the most precise lunar coordinate system to date. The given formal errors, however, may be too optimistic. Table 4 shows that, while the differences between positions determined in the four obtained solutions are 15 cm or less, the differences with DE430 [77, Table 6] or INPOP17a [69] positions reach 2 m.

**Table 3** Determined positions of five reference points in PA selenocentric coordinate system.

Panel	$X$ , m	$Y$ , m	$Z$ , m	$\sigma X$ , cm	$\sigma Y$ , cm	$\sigma Z$ , cm
Apollo 11	1591967.619	690697.773	21004.477	3.1	2.0	0.8
Apollo 14	1652689.300	-520999.332	-109729.671	3.1	2.1	0.8
Apollo 15	1554678.256	98093.848	765006.089	3.0	1.9	1.7
Luna 17	1114291.065	-781299.633	1076059.333	3.0	1.7	2.0
Luna 21	1339364.109	801870.501	756359.405	3.0	1.9	1.7

**Table 4** For each of the five reference points: maximum pairwise distance between its positions in the four obtained solutions; maximum distance between its positions in the obtained solutions and its position in the DE430 solution; maximum distance between its positions in the obtained solutions and its position in the INPOP17a solution.

Panel	Max $\Delta$ btw solutions	Max $\Delta$ DE430	Max $\Delta$ INPOP17a
Apollo 11	0.15 m	2.1 m	2.3 m
Apollo 14	0.11 m	2.0 m	2.2 m
Apollo 15	0.13 m	1.8 m	2.2 m
Luna 17	0.15 m	1.7 m	2.2 m
Luna 21	0.15 m	1.7 m	1.9 m

## 5.2 Planetary part

In the planetary solution the following parameters were determined:

- Three angles of orientation with respect to ICRF;
- Planetary orbital elements at epoch, including Pluto. For Earth, only the eccentricity, semimajor axis and longitude of the periapsis were determined to avoid correlations with the three ICRF angles;
- Solar oblateness factor;
- Gravitational parameters of the Sun, some individual asteroids and TNOs;
- Total gravitational parameters of asteroids of C, S, M taxonomic classes, asteroid belt and Kuiper belt (apart from asteroids/TNOs whose masses were fixed to known values or determined individually);
- Rotational parameters of Mars;
- Parameters of Mercury topography;
- Locations of Martian landers Viking 1/2 and Pathfinder;
- Solar corona electron density factors (one per each solar conjunction, assuming a symmetric  $1/r^2$  distribution)
- Shifts to compensate calibration errors or clock offsets on Earth or in spacecraft;
- Phase effects for optical observations of outer planets.

For details about the planetary part of EPM ephemeris, the reader is referred to [56, 59, 58, 60].

The whole Solar system was oriented to ICRF via single-baseline and multiple-baseline  $\Delta$ DOR observations. While multiple-baseline observations are given as the direct astrometrical position  $(\alpha, \delta)$  of a planet, the single-baseline ones are given as a single observable  $\Delta\theta$ . That observable is a linear combination of differences  $(\Delta\alpha, \Delta\delta)$  between the astrometrical of the planet and its position in the DE405 ephemeris:

$$\Delta\theta = \Delta\alpha \cos \gamma + \Delta\delta \cos \alpha \sin \gamma,$$

where  $\gamma$  is the angle of VLBI baseline on plane of sky, relative to celestial equator.

After orientation to ICRF, the following residuals were obtained: Figs. 1 and 2 for Venus, Mars, and Jupiter single-baseline VLBI observables; Figs. 3

and 4 for Saturn and Mars astrometric positions obtained by VLBA observations.

The formal errors ( $1\sigma$ ) of the three angles of rotation (around X, Y, and Z axes) of ephemeris frame to ICRF were the following:  $\sigma(\Delta X) = 0.038$  mas,  $\sigma(\Delta Y) = 0.041$  mas,  $\sigma(\Delta Z) = 0.024$  mas.

The rotational trends ( $\dot{X}$ ,  $\dot{Y}$ ,  $\dot{Z}$ ) were once temporarily added into the set of the determined parameters, and were found to be below their respective  $1.5\sigma$ , where  $\sigma(\dot{X}) = 14 \mu\text{as}/\text{year}$ ,  $\sigma(\dot{Y}) = 15 \mu\text{as}/\text{year}$ , and  $\sigma(\dot{Z}) = 9 \mu\text{as}/\text{year}$ . That proves that the dynamical planetary model of the ephemeris properly accounts for all natural phenomena that can have a rotational effect on the Solar system within the given error margin. Estimates of the galactic aberration are below that margin, at 5–10  $\mu\text{as}/\text{year}$  [33,38].

## 6 Determination of daily corrections to rotational parameters of Earth and Moon

An LLR session running for several hours allows to determine two daily (nightly) parameters of Earth rotation: UT0 and VOL, which are in linear relation with UT1 and terrestrial pole coordinates  $x_p$ ,  $y_p$  [6]:

$$\begin{aligned} \text{UT0} &= \text{UT1} + \frac{(x_p \sin \lambda + y_p \cos \lambda) \tan \phi}{15 \times 1.002737909} \\ \text{VOL} &= x_p \cos \lambda - y_p \sin \lambda \end{aligned}$$

where  $\lambda$  and  $\phi$  are the station's longitude and latitude, respectively, and 1.002737909 is the relative rate of mean solar time to sidereal time. Without the LLR sessions happening in two observatories on one night (which is rare), there is no possibility to determine daily UT1,  $x_p$ , and  $y_p$  from LLR alone.

Lunar laser ranging is usually performed to more than one lunar target (retroreflector). That allows to determine two lunar orientation parameters:  $r'$  and  $q'$ . LLR is not sensitive to the third parameter,  $p'$  — the angle of rotation around the X axis, directed towards the Earth.

### 6.1 Setting of experiment

Once the ephemeris, obtained with C04 as the EOP series, has been fixed, a special LLR solution was obtained, containing five determined parameters for each night with 10 or more LLR normal points:  $\Delta\text{UT0}$ , VOL,  $r'$ ,  $q'$ , and range error  $\Delta r$ . The range error is assumed to originate from imperfections of the troposphere model and the lunar orbital ephemeris and correlates with  $\Delta\text{UT0}$  and VOL. The inclusion of the range error into the set allows to obtain realistic error estimates for the EOP parameters.

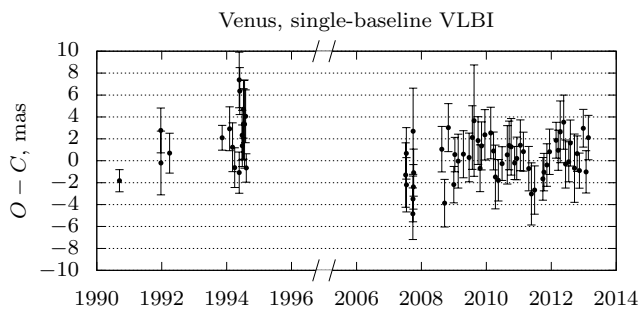


**Fig. 1** Postfit residuals of single-baseline VLBI observable  $\Delta\theta$  for Venus orbiters Magellan and Venus Express.

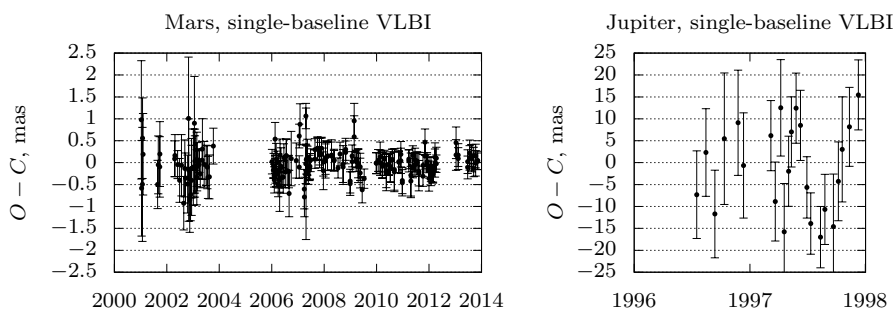


**Fig. 2** Postfit residuals of single-baseline VLBI observable  $\Delta\theta$  for Mars orbiters MGS, Odyssey, and MRO, and Jupiter orbiter Galileo

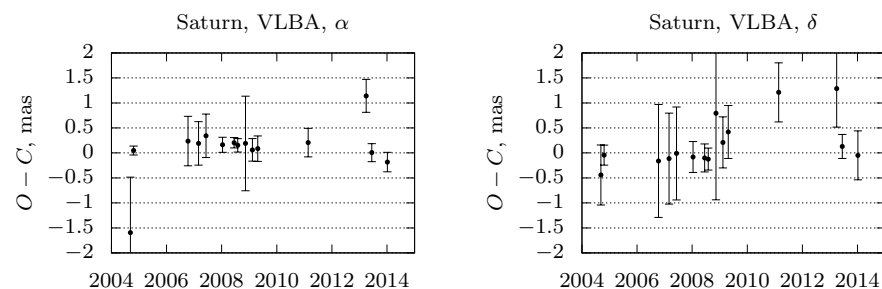


**Fig. 3** Postfit residuals of astrometric positions of Saturn obtained on VLBA observations of Cassini spacecraft.

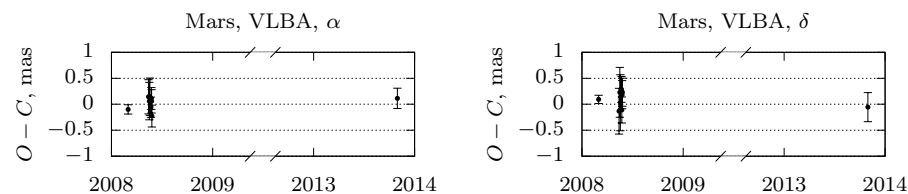


**Fig. 4** Postfit residuals of astrometric positions of Mars obtained on VLBA observations of MRO and Odyssey spacecraft.

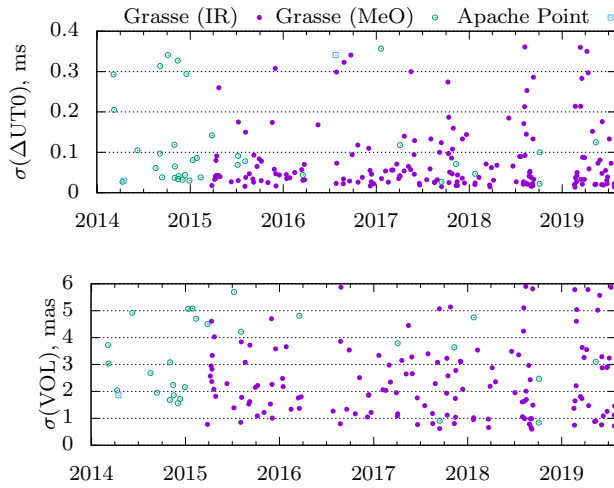


**Fig. 5** Formal errors of UT0 and VOL determined from LLR since 2014.

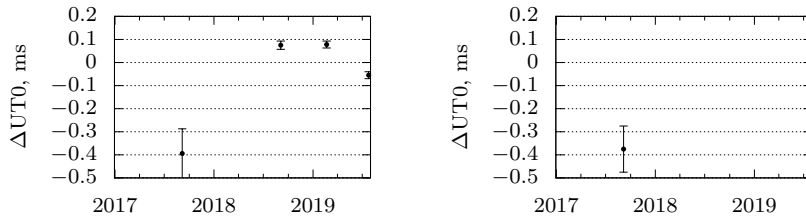


**Fig. 6**  $\Delta\text{UT0}$  values detected by Grasse infrared laser outside  $3\sigma$  w.r.t. C04 series (left) and “finals” (right).

## 6.2 Results

The results are shown for the timespan of January 2014 – July 2019 for three instruments at two observatories. There were 340 sessions altogether with 10 or more normal points. There has not been such an LLR session at Wettzell observatory in that timespan. On the plots, only the results with formal errors ( $1\sigma$ ) below 6 mas are shown. Fig. 5 shows the formal errors of determined UT0 and VOL.

There are 173 nights with  $\sigma(\Delta\text{UT0})$  below 1.5 mas (0.1 ms) and 50 nights with  $\sigma(\text{VOL})$  below 1.5 mas. Almost all determined corrections are within their  $3\sigma$  range. The outliers—four UT0 corrections w.r.t. C04 series and one w.r.t. “finals”—are shown at Fig. 6. For C04, their values and formal errors are:  $-394 \pm 107\mu\text{s}$  (6 Sep 2017),  $75 \pm 18\mu\text{s}$  (4 Sep 2018),  $78 \pm 15\mu\text{s}$  (20 Feb 2019),  $81 \pm 16\mu\text{s}$  (4 Sep 2019), and  $-55 \pm 15\mu\text{s}$  (25 Jul 2019). The only outlier for “finals” is  $-375 \pm 100\mu\text{s}$  (6 Sep 2017).

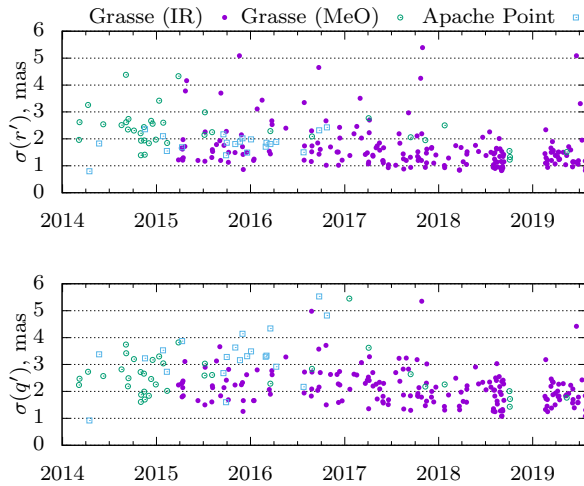


**Fig. 7** Formal errors of  $r'$  and  $q'$  determined from LLR since 2014.

The absence of the other three outliers in the UT0 corrections w.r.t. “finals” further supports the inference that the “finals” series represent the actual rotation of the Earth slightly better than C04 at present and that the LLR can sense it.

The single outlier common to both series can indicate either an Earth rotation event not determined by daily VLBI observations, or an artifact in Grasse data on that day. In any case, LLR will probably have a non-negligible effect on modern IERS EOP solutions, and even more so when other LLR observatories, like Wettzell, begin to provide frequent infrared data.

Fig. 7 shows the formal errors of  $r'$  and  $q'$  for nights where those errors are below 6 mas. Data on Figs. 5 and 7 come not from separate solutions but from single solution, where the range errors were also determined. The range errors are not shown. All determined  $p'$  and  $q'$  are within their  $3\sigma$  range.

## 7 Determination of orientation of ephemeris frame in the ICRF from LLR data

In planetary ephemerides, orbits of planets, including Earth, are determined in a so-called barycentric celestial reference frame (BCRF [30]), also known as ephemeris frame. Like ICRF, it is defined to have its origin at the barycenter of the Solar system. It is also defined to be an inertial frame. It is important to tie dynamical BCRF to the kinematic ICRF as precisely as possible, for three applications:

- Modeling the orbits of interplanetary spacecraft;
- Studying the influence of the Moon, planets, and the Sun to the rotation of the Earth;

- Supporting astronomical instruments on other planets and the Moon (in the future).

Probably the earliest tie between the ephemeris and radio frame based on quasars was made in 1986 [47], long before the official adoption of ICRF in 1998. The tie was based on  $\Delta$ DOR observations of Viking and Pioneer spacecraft; the accuracy was about 20 mas. Later, the accuracy of the tie was improved to about 5 mas [15], and then to 3 mas [20] by using a different approach: processing LLR together with quasar VLBI observations. However, in subsequent years, the abundance of a higher quality  $\Delta$ DOR observations of spacecraft, including those of Magellan (since 1990), quickly led back to the decision to use just  $\Delta$ DOR for the direct ephemeris-ICRF tie [66]. In DE405 ephemeris [65] (1998), a 1 mas accuracy of the tie was reported. Similar result was obtained in EPM2002 ephemeris [55].

The modern ephemerides DE430 [19, 17] and EPM2017 [57, 58] have their tie to ICRF based on modern spacecraft VLBI measurements, with accuracy of about 0.2 mas. As for INPOP ephemerides, the 0.5 mas accuracy of the tie was reported for an older version INPOP13 [14]. The LLR data is not used for that tie; however, the lunar solution in DE430 [17, 77] contains four corrections to IAU1980 nutation model, namely:

- X-axis rotation at J2000 and its rate, “obliquity rate”
- Y-axis rotation at J2000 and its rate, “luni-solar precession”

In DE430, those corrections are not used outside the lunar solution, and particularly, are not used for ephemeris-ICRF frame tie determination.

Similar four corrections (but to IAU2000 nutation model rather than to IAU1980) were obtained in [23]. The corrections were treated as *the* “tie between the dynamical ephemeris frame to the kinematic celestial frame”; no spacecraft VLBI data were considered.

In this work, the two methods of obtaining BCRF–ICRF tie are applied and their results are compared. Fig. 8 shows the (seemingly) redundant scheme to tie planetary orbits to ICRF. The direct “orbits–ICRF” connector is what is normally used in ephemerides. At the same time, the orbits of planets are tied to the ecliptic in the ephemeris, via spacecraft ranging (most precise technique), and also differenced range observations of spacecraft and optical observations of planets and their satellites. The ecliptic is connected to the equator via LLR. The equator, in turn, is tied to the ICRF via VLBI observations of quasars.

## 7.1 Setting of experiment

Planetary solution (see Sec. 5) was obtained and its frame tied to the ICRF using spacecraft VLBI observations. Then, the lunar solution was re-obtained, with eight more parameters from (3):  $\Delta X, \Delta Y, \dot{X}, \dot{Y}, C_X^\Omega, S_X^\Omega, C_Y^\Omega$  and  $S_Y^\Omega$ . (The  $\Delta Z$  rotation can not be determined as long as the positions of the stations are determined in the solution.) These parameters, per se, have no relation to

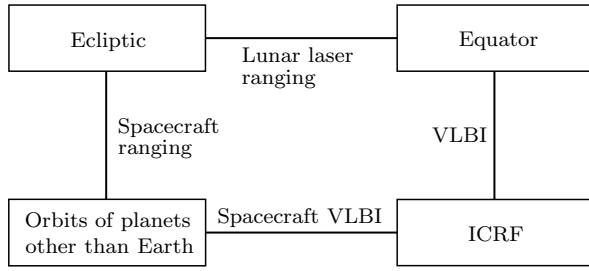


**Fig. 8** Different ties realised with different techniques.

planets; we call them the tie between the dynamical Earth–Moon system and the ICRF. The procedure is repeated four times: for C04 and “finals” EOP series, and for DE430 and IERS models of tidal variations of geopotential.

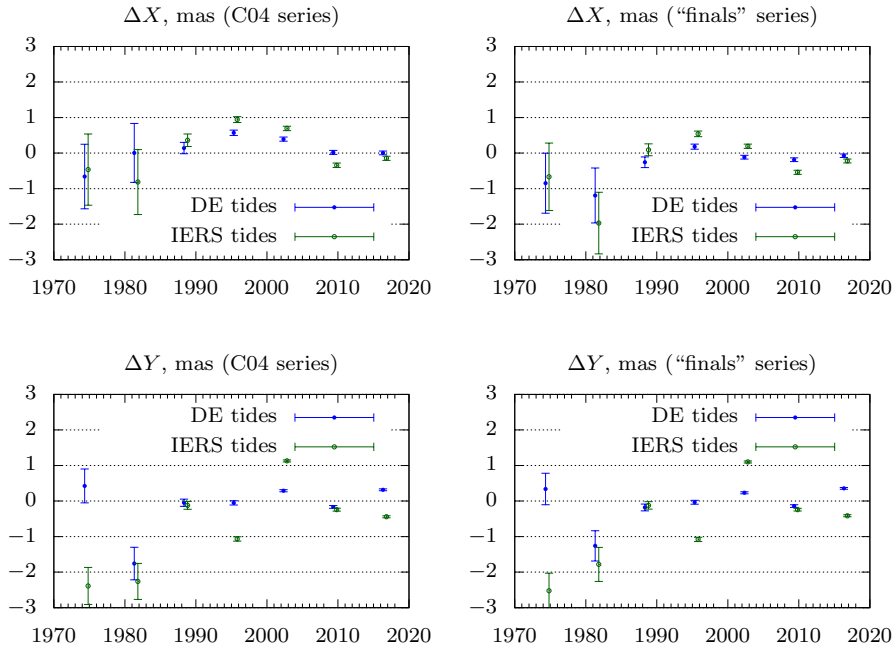
## 7.2 Results and discussion

Table 5 shows the determined rotations, their trends and 18.6-year amplitudes. It is visible that the values vary greatly across the four solutions. In particular, the strong  $\dot{X}$  trend is detected in all solutions but one. The strong  $\dot{Y}$  trend is detected in two solutions. There is not one solution where both trends are low. That fact alone makes the determined constant rotations irrelevant; the trends must be explained first. The same applies to the determined amplitudes. It is visible that they are all big with the IERS tidal model; also, neither of the two solutions based on the DE430 tidal model has low values of all the four amplitudes.

**Table 5** Ephemeris-ICRF rotation angles, their rates and 18.6 year amplitudes, determined from LLR. The four columns of numbers are the combinations of two geopotential variations models (DE430 and IERS2010) and two IERS EOP series (C04 and “finals”). The given errors are  $1\sigma$ .

	DE430 tides		IERS2010 tides	
	C04	finals	C04	finals
$\Delta X_0$ , mas	$0.375 \pm 0.049$	$-0.050 \pm 0.046$	$0.221 \pm 0.055$	$-0.184 \pm 0.052$
$\Delta Y_0$ , mas	$0.011 \pm 0.026$	$0.052 \pm 0.024$	$0.287 \pm 0.029$	$0.279 \pm 0.027$
$\dot{X}$ , $\mu\text{as}/\text{year}$	$-30.1 \pm 4.1$	$-13.5 \pm 3.8$	$-14.1 \pm 4.6$	$2.1 \pm 4.3$
$\dot{Y}$ , $\mu\text{as}/\text{year}$	$10.9 \pm 2.2$	$12.4 \pm 2.0$	$-14.4 \pm 2.9$	$-14.1 \pm 2.3$
$C_X^\Omega$ , mas	$-0.026 \pm 0.039$	$-0.291 \pm 0.037$	$-0.620 \pm 0.042$	$-0.663 \pm 0.040$
$S_X^\Omega$ , mas	$-0.228 \pm 0.034$	$-0.260 \pm 0.031$	$0.465 \pm 0.037$	$0.457 \pm 0.035$
$C_Y^\Omega$ , mas	$0.102 \pm 0.026$	$0.018 \pm 0.025$	$0.505 \pm 0.030$	$0.414 \pm 0.028$
$S_Y^\Omega$ , mas	$-0.033 \pm 0.036$	$0.026 \pm 0.033$	$0.329 \pm 0.039$	$0.388 \pm 0.036$

To further study the temporal behavior of the ICRF tie, four other lunar solutions were obtained—without the determined trends or amplitudes, but rather with seven pairs of  $(\Delta X, \Delta Y)$ , each affecting a seven-year timespan of



**Fig. 9** Piecewise ties for dynamical Earth–Moon system to ICRF.  $\Delta X$  and  $\Delta Y$  corrections for different combinations of EOP series (C04/finals) and geopotential variations model (DE430/IERS2010) are shown. Each point represents a seven-year timespan (starting and ending on 1 May); IERS tides points have been artificially moved to the right for clarity.

LLR observations. In total, the “piecewise tie” to ICRF was calculated for the timespan of 49 years (from 1 Aug 1970 to 1 Aug 2019).

Figure 9 shows the piecewise ICRF tie  $\Delta X$  and  $\Delta Y$  corrections. The baseline of the plots corresponds to the lunar-planetary ephemeris oriented to ICRF via  $\Delta DOR$  observations (see Figs. 1–4). It is clear that there are systematic differences between the ties depending on the used tidal model, EOP series, and time. Until those issues are resolved, in the requirement of sub-mas accuracy, the LLR observations are of no help for the BCRF–ICRF tie. However, the obtained result is interesting by itself because it indicates deeper problems with the assumptions that were made on Fig. 8.

One problem is the EOP series. Table 5 and Fig. 9 clearly show that the tie between the Earth–Moon system and the ICRF suffers from absence of sub-mas agreement in the celestial pole trend, let alone its position, between C04 and “finals” series. The disagreement in celestial pole series has been studied before [37, 40, 39]. For instance, [37, Table 3] shows  $dX$  slope for C04 and “finals” series at  $15.1 \pm 1.8 \mu\text{as}/\text{year}$  and  $1.1 \pm 1.6 \mu\text{as}/\text{year}$ , respectively. So the difference is outside the error margin. For  $dY$  slope, the values are  $59.6 \pm 1.8$  and  $50.9 \pm 1.7 \mu\text{as}/\text{year}$ . The difference between those slopes is not as big as with  $dX$  slopes, but there is another problem: the values are

**Table 6** Assumptions about models and frames, and comments on validity on those assumptions on sub-mas level.

Assumption	Validity
ICRF forms an inertial frame	True (apart from the galactic aberration which is estimated at 5–10 $\mu\text{as}/\text{year}$ )
Dynamic frame of planets is inertial	True (mathematically)
Dynamic model of planets accounts for all natural phenomena that can have a rotational effect on the Solar system detectable by present observations	Probably true. One problem in that regard may come from inaccurate value of Sun's $J_2$ , however it is well determined from MESSENGER observations. Also, the planetary solution does not detect rotation from spacecraft VLBI observations at the level of few tens $\mu\text{as}/\text{year}$ .
Celestial pole coordinates are known from VLBI observations	False, as shown in [37, 40, 39]
Dynamical frame of the Earth–Moon system is inertial	Unknown, because of the involved non-dynamical models of Earth gravitational potential and Earth rotation with EOP
Dynamical model of the Earth–Moon system accounts for all natural phenomena that can have a rotational effect on the real Earth–Moon system detectable by present observations	Probably false, since different models of geopotential already produce different rotational effects, as shown in Table 5 and Fig. 9.

bigger than any  $dY$  slope obtained from the single VLBI series constituting the combined series.

The second problem is the lunar model. Different model values of Earth's  $J_2$  and different models of tidal variations of that value can cause different rotational behavior of the Earth–Moon system. The difference between DE430 model and IERS2010 model is clearly visible in Fig. 9 and Table 5: for instance,  $\dot{Y}$  has different signs depending on the model; also, 18.6-year amplitudes are always strongly detected with the IERS2010 model, while some of them are not detected with the DE430 model.

The assumptions and comments on their validity are summarized in Table 6. With present state of lunar model, and with present state of celestial pole EOP series, one can not rely on either of those things to verify the other. Further development of methods for EOP solutions, and further development of Earth–Moon dynamical model are needed—whichever happens first, will help to solve problems with the other.

## Conclusion

- OCA observatory (former CERGA) in Grasse, France continues to provide large amounts of LLR green and infrared data. Matera observatory in Italy provides infrequent LLR data. Wettzell observatory started to provide LLR infrared data of a very good quality.
- LLR was useful for building EOP series in the past. Modern LLR, too, is able to detect inaccuracies in modern EOP series, with sub-mas accuracy.

Probably the LLR data can benefit combined EOP solutions; currently it is used in KEOF, which does not include celestial pole.

- LLR is capable of detecting two out of three lunar orientation parameters (LOPs) with accuracy of few mas. However, on the present data, no statistically significant daily deviations of LOPs from the lunar rotational model were detected. The lunar model research should continue, though, in the area of long-term variations.
- The tie between ephemeris frame and ICRF, calculated from spacecraft VLBI ( $\Delta$ DOR) data, is confirmed with the latest data with the accuracy of 0.18 mas ( $3\sigma$ ).
- IERS Bulletin A weekly EOP series produce generally better fits of LLR solutions than IERS C04.
- LLR is potentially capable of tying the Earth–Moon system to ICRF (and hence, the whole ephemeris frame to ICRF) with accuracy comparable to that of  $\Delta$ DOR-based tie; however, one obstacle is the location of the celestial pole in EOP series: it is not accurate enough to use the equator–ICRF link to tie the ecliptic to ICRF via LLR observations and their ecliptic–equator link.
- More research is needed in the area of Earth–Moon dynamical system, and particularly in the model of geopotential which affects the lunar orbital motion. Two available models (IERS2010 and DE430) produce different rotational rates of the Earth–Moon system in the celestial frame, which is detectable by LLR observations. The research of the Earth–Moon dynamics will be facilitated by an improvement in present celestial pole series (or vice versa).

**Acknowledgements** Author would like to thank his colleagues: Elena Pitjeva for her continuous support and particular help with the spacecraft VLBI topic, and Sergey Kurdubov for much helpful advice throughout this work.

This work would not have been possible without the effort of personnel at observatories doing lunar laser ranging, particularly Tom Murphy in Apache Point, Etienne Samain and Jean-Marie Torre in Grasse, Giuseppe Bianco in Matera, Karl Ulrich Schreiber in Wettzell, Peter Shelus in McDonald, Walter Bonsack in Haleakala, and Andrei Severny in Nauchny.

The POLAC website was of great help, where Christophe Barache, Sébastien Bouquillon, Teddy Carlucci, and Gerard Francou carefully collected LLR observations from different sources.

Planetary observations, including spacecraft VLBI which is essential for part of this work, were collected at the NASA SSD webpage and are supported by William Folkner, and at the Geoazur website supported by Agnès Fienga.

Anonymous reviewers provided useful advice which allowed to significantly improve the paper.

**Author contributions** D. P. designed and performed the research and wrote the manuscript.

**Data availability** All the observational data used in this work comes from publicly available sources listed in section 2. The EOP series are publicly available at the IERS website <http://iers.org>.

## References

1. Aksim, D., Pavlov, D.: On the extension of Adams–Bashforth–Moulton Methods for numerical integration of delay differential equations and application to the Moon’s orbit (2019). URL <https://arxiv.org/pdf/1903.02098>
2. Araki, H., Kashima, S., Noda, H., Kunimori, H., Chiba, K., Mashiko, H., Kato, H., Otsubo, T., Matsumoto, Y., Tsuruta, S., Asari, K., Hanada, H., Yasuda, S., Utsunomiya, S., Takino, H.: Thermo-optical simulation and experiment for the assessment of single, hollow, and large aperture retroreflector for lunar laser ranging. *Earth, Planets and Space* **68**(1), 101 (2016). DOI 10.1186/s40623-016-0475-4
3. Biskupek, L., Müller, J., Hofmann, F.: Determination of nutation coefficients from lunar laser ranging. In: S. Kenyon, M.C. Pacino, U. Marti (eds.) *Geodesy for Planet Earth*, pp. 521–525. Springer Berlin Heidelberg, Berlin, Heidelberg (2012). DOI 10.1007/978-3-642-20338-1\_63
4. Bizouard, C., Lambert, S., Becker, O., Richard, J.Y.: The combined solution C04 for Earth Rotation Parameters consistent with International Terrestrial Reference Frame 2014. Preliminary draft, Observatoire de Paris, SYRTE (2011). URL <http://hpiers.obspm.fr/iers/eop/eopc04/C04.guide.pdf>
5. Bonsack, W.K., Macknik, L.S., Dawe, R.S.: Lunar and satellite ranging from Haleakala, Maui. Publications of the Astronomical Society of the Pacific **98**, 1102 (1986)
6. Chapront, J., Francou, G.: Lunar laser ranging analysis: determination of UT0 and VOL. Tech. rep., Observatoire de Paris, SYRTE department (2009). URL [ftp://cyrano-se.obspm.fr/pub/1\\_llr\\_analysis/3\\_fitted\\_parameters/doc7.pdf](ftp://cyrano-se.obspm.fr/pub/1_llr_analysis/3_fitted_parameters/doc7.pdf)
7. Chapront, J., Chapront-Touzé, M., Francou, G.: A new determination of lunar orbital parameters, precession constant and tidal acceleration from LLR measurements. *A&A* **387**(2), 700–709 (2002). DOI 10.1051/0004-6361:20020420
8. Charlot, P. (ed.): Earth orientation, reference frames and atmospheric excitation functions submitted for the 1994 IERS Annual Report. Central Bureau of IERS — Observatoire de Paris, Paris (1995). URL <https://www.iers.org/SharedDocs/Publikationen/EN/IERS/Publications/tn/TechnNote19/tn19.pdf>. IERS Technical Note 19
9. Courde, C., Torre, J.M., Samain, E., Martinot-Lagarde, G., Aymar, M., Albanese, D., Exertier, P., Fienga, A., Marley, H., Metris, G., Viot, H., Viswanathan, V.: Lunar laser ranging in infrared at the Grasse laser station. *A&A* **602**, A90 (2017). DOI 10.1051/0004-6361/201628590
10. Currie, D., Dell’Agnello, S., Monache, G.D.: A lunar laser ranging retroreflector array for the 21st century. *Acta Astronautica* **68**(7), 667 – 680 (2011). DOI 10.1016/j.actaastro.2010.09.001
11. Dick, W.R., Thaller, D. (eds.): *IERS Annual Report 2017*. Verlag des Bundesamts für Kartographie und Geodäsie, Frankfurt am Main (2018). URL <https://www.iers.org/SharedDocs/Publikationen/EN/IERS/Publications/ar/ar2017/ar2017.pdf>
12. Dickey, J.O., Newhall, X.X., Williams, J.G.: Earth orientation from lunar laser ranging and an error analysis of polar motion services. *Journal of Geophysical Research: Solid Earth* **90**(B11), 9353–9362 (1985). DOI 10.1029/JB090iB11p09353
13. Felleisen, M., Findler, R.B., Flatt, M., Krishnamurthi, S., Barzilay, E., McCarthy, J., Tobin-Hochstadt, S.: A programmable programming language. *Commun. ACM* **61**(3), 62–71 (2018). DOI 10.1145/3127323
14. Fienga, A., Laskar, J., Gastineau, M., Verma, A.: INPOP new release: INPOP13c. Tech. rep., Observatoire de Paris (2013). URL <http://www.imcce.fr/fr/presentation/equipes/ASD/inpop/inpop13c.pdf>
15. Finger, M.H., Folkner, W.M.: A determination of the radio-planetary frame tie from comparison of Earth orientation parameters. The telecommunications and data acquisition progress report 42-109, NASA JPL (1992). URL [https://ipnpr.jpl.nasa.gov/progress\\_report/42-109/109A.PDF](https://ipnpr.jpl.nasa.gov/progress_report/42-109/109A.PDF)
16. Flatt, M., PLT: Reference: Racket. Tech. Rep. PLT-TR-2010-1, PLT Design Inc. (2010). URL <http://racket-lang.org/tr1>
17. Folkner, W., Williams, J., Boggs, D., Park, R., Kuchynka, P.: The Planetary and Lunar Ephemerides DE430 and DE431. IPN Progress Report 42-196, NASA JPL (2014). URL [http://naif.jpl.nasa.gov/pub/naif/generic\\_kernels/spk/planets/de430\\_and\\_de431.pdf](http://naif.jpl.nasa.gov/pub/naif/generic_kernels/spk/planets/de430_and_de431.pdf)

18. Folkner, W.M.: Planetary ephemeris DE423 fit to Messenger encounters with Mercury. IOM 343R-10-001, NASA JPL (2010). URL [https://naif.jpl.nasa.gov/pub/naif/generic\\_kernels/spk/planets/a\\_old\\_versions/de423\\_for\\_mercury\\_and\\_venus/de423.iom.pdf](https://naif.jpl.nasa.gov/pub/naif/generic_kernels/spk/planets/a_old_versions/de423_for_mercury_and_venus/de423.iom.pdf)
19. Folkner, W.M., Border, J.S.: Linking the planetary ephemeris to the International Celestial Reference Frame. Proceedings of the International Astronomical Union **10**(H16), 219220 (2012). DOI 10.1017/S1743921314005493
20. Folkner, W.M., Charlot, P., Finger, M.H., Williams, J.G., Sovers, O.J., Newhall, X., Standish Jr., E.M.: Determination of the extragalactic-planetary frame tie from joint analysis of radio interferometric and lunar laser ranging measurements. *Astronomy and Astrophysics* **287**, 279–289 (1994)
21. Folkner, W.M., Yoder, C.F., Yuan, D.N., Standish, E.M., Preston, R.A.: Interior structure and seasonal mass redistribution of Mars from radio tracking of Mars Pathfinder. *Science* **278**(5344), 1749–1752 (1997). DOI 10.1126/science.278.5344.1749
22. Hildebrand, C.E., Iijima, B.A., Kroger, P.M., Folkner, W.M., Edwards, C.D.: Radio-planetary frame tie from Phobos-2 VLBI data. Telecommunications and data acquisition progress report 42-119, NASA JPL (1994)
23. Hofmann, F., Biskupek, L., Müller, J.: Contributions to reference systems from lunar laser ranging using the IFE analysis model. *Journal of Geodesy* **92**(9), 975–987 (2018). DOI 10.1007/s00190-018-1109-3
24. Hofmann, F., Müller, J.: Relativistic tests with lunar laser ranging. *Classical and Quantum Gravity* **35**(3), 035015 (2018). DOI 10.1088/1361-6382/aa8f7a
25. Hofmann, F., Müller, J., Biskupek, L.: Lunar laser ranging test of the Nordtvedt parameter and a possible variation in the gravitational constant. *A&A* **522**, L5 (2010). DOI 10.1051/0004-6361/201015659
26. Hohenkerk, C.: SOFA and the algorithms for transformations between time scales and between reference systems. In: H. Schuh, S. Böhm, T. Nilsson, N. Capitaine (eds.) Proceedings of the Journées 2011 “Systèmes de référence spatio-temporels”, pp. 21–24. Vienna University of Technology (2012)
27. Hugentobler, U., Neidhardt, A., Lauber, P., Ettl, M., Schreiber, K.U., Dassing, R., Klügel, T., Riepl, S., Herold, G., Kronschnabl, G., Plötz, C., Hessels, U.: The Geodetic Observatory Wettzell—A fundamental reference point. In: Geological Field Trips in Central Western Europe. Geological Society of America (2011). DOI 10.1130/2011.0022(01)
28. Jones, D.L., Folkner, W.M., Jacobson, R.A., Jacobs, C.S., Dhawan, V., Romney, J., Fomalont, E.: Astrometry of Cassini with the VLBA to improve the Saturn ephemeris. *The Astronomical Journal* **149**(1) (2014). DOI 10.1088/0004-6256/149/1/28
29. Konopliv, A.S., Asmar, S.W., Folkner, W.M., Karatekin, O., Nunes, D.C., Smrekar, S.E., Yoder, C.F., Zuber, M.T.: Mars high resolution gravity fields from MRO, Mars seasonal gravity, and other dynamical parameters. *Icarus* **211**(1), 401–428 (2011). DOI 10.1016/j.icarus.2010.10.004
30. Kopeikin, S., Efroimsky, M., Kaplan, G.: *Relativistic Celestial Mechanics of the Solar System*. Wiley-VCH Verlag GmbH & Co. KGaA (2011). DOI 10.1002/9783527634569
31. Kopeikin, S.M.: Theory of Relativity in Observational Radio Astronomy. *Sov. Astron.* **34**(1), 5–9 (1990)
32. Kuchynka, P., Folkner, W.M., Konopliv, A.S.: Station-Specific Errors in Mars Ranging Measurements. Interplanetary network progress report 42-190, NASA JPL (2012). URL [https://ipnpr.jpl.nasa.gov/progress\\_report/42-190/190C.pdf](https://ipnpr.jpl.nasa.gov/progress_report/42-190/190C.pdf)
33. Kurdubov, S.: Estimation of Solar system acceleration from VLBI. In: W. Alef, S. Bernhart, A. Nothnagel (eds.) Proceedings of the 20th Meeting of the European VLBI Group for Geodesy and Astronomy, pp. 112–113. Universität Bonn (2011). URL [http://www.oso.chalmers.se/evga/20\\_EVGA\\_2011\\_Bonn.pdf](http://www.oso.chalmers.se/evga/20_EVGA_2011_Bonn.pdf)
34. Kurdubov, S.L., Pavlov, D.A., Mironova, S.M., Kaplev, S.A.: Earth–Moon very-long-baseline interferometry project: modelling of the scientific outcome. *Monthly Notices of the Royal Astronomical Society* **486**(1), 815–822 (2019). DOI 10.1093/mnras/stz827
35. Langley, R.B., King, R.W., Shapiro, I.I.: Earth rotation from lunar laser ranging. *Journal of Geophysical Research: Solid Earth* **86**(B12), 11913–11918 (1981). DOI 10.1029/JB086iB12p11913

36. Luzum, B., Capitaine, N., Fienga, A., Folkner, W., Fukushima, T., Hilton, J., Hohenkerk, C., Krasinsky, G., Petit, G., Pitjeva, E., Soffel, M., Wallace, P.: The IAU 2009 system of astronomical constants: the report of the IAU working group on numerical standards for fundamental astronomy. *Celestial Mechanics and Dynamical Astronomy* **110**(4), 293 (2011). DOI 10.1007/s10569-011-9352-4
37. Malkin, Z.: Celestial pole offsets: From initial analysis to end user. In: D. Behrend, K.D. Baver (eds.) *IVS 2012 General Meeting Proceedings*, pp. 375–379. NASA GSFC (2012). URL <http://ivsc.gsfc.nasa.gov/publications/gm2012/malkin.pdf>
38. Malkin, Z.: On the implications of the Galactic aberration in proper motions for the Celestial Reference Frame. *Monthly Notices of the Royal Astronomical Society* **445**(1), 845–849 (2014). DOI 10.1093/mnras/stu1796
39. Malkin, Z.: Joint analysis of celestial pole offset and free core nutation series. *Journal of Geodesy* **91**(7), 839–848 (2017). DOI 10.1007/s00190-016-0966-x
40. Malkin, Z.M.: On the accuracy of the theory of precession and nutation. *Astronomy Reports* **58**(6), 415–425 (2014). DOI 10.1134/s1063772914060043
41. Matsumoto, K., Yamada, R., Kikuchi, F., Kamata, S., Ishihara, Y., Iwata, T., Hanada, H., Sasaki, S.: Internal structure of the moon inferred from Apollo seismic data and selenodetic data from GRAIL and LLR. *Geophysical Research Letters* **42**(18), 7351–7358 (2015). DOI 10.1002/2015GL065335
42. Mendes, V.B., Pavlis, E.C.: High-accuracy zenith delay prediction at optical wavelengths. *Geophysical Research Letters* **31**(14) (2004)
43. Mendes, V.B., Prates, G., Pavlis, E.C., Pavlis, D.E., Langley, R.B.: Improved mapping functions for atmospheric refraction correction in SLR. *Geophysical Research Letters* **29**(10), 53–1–53–4 (2002)
44. Morley, T., Budnik, F.: Mars Express and Venus Express range residuals for improving planetary ephemerides. In: *21st International Symposium on Space Flight Dynamic (2009)*. URL [http://issfd.org/ISSFD\\_2009/OrbitDeterminationI/Morley.pdf](http://issfd.org/ISSFD_2009/OrbitDeterminationI/Morley.pdf)
45. Murphy, T.: Lunar laser ranging: the millimeter challenge. *Rep. Prog. Phys.* **76**, 076901 (2013)
46. Murphy, T., Adelberger, E., Battat, J., Hoyle, C., Johnson, N., McMillan, R., Stubbs, C., Swanson, H.: APOLLO: millimeter lunar laser ranging. *Class. Quantum Grav.* **29**, 184005 (2012)
47. Newhall, X.X., Preston, R.A., Esposito, P.B.: Relating the JPL VLBI reference frame and the planetary ephemerides. *Symposium - International Astronomical Union* **109**, 789–794 (1986). DOI 10.1017/S0074180900077330
48. Park, R.S., Folkner, W.M., Jones, D.L., Border, J.S., Konopliv, A.S., Martin-Mur, T.J., Dhawan, V., Fomalont, E., Romney, J.D.: Very Long Baseline Array astrometric observations of Mars orbiters. *The Astronomical Journal* **150**(4) (2015). DOI 10.1088/0004-6256/150/4/121
49. Park, R.S., Folkner, W.M., Konopliv, A.S., Williams, J.G., Smith, D.E., Zuber, M.T.: Precession of Mercury’s perihelion from ranging to the MESSENGER spacecraft. *The Astronomical Journal* **153**(3) (2017). DOI 10.3847/1538-3881/aa5be2
50. Pavlov, D., Skripnichenko, V.: Rework of the ERA software system: ERA-8. In: Z. Malkin, N. Capitaine (eds.) *Proceedings of the Journées 2014 “Systèmes de référence spatio-temporels”*, pp. 243–246. Pulkovo Observatory (2015)
51. Pavlov, D., Williams, J., Suvorkin, V.: Determining parameters of Moon’s orbital and rotational motion from LLR observations using GRAIL and IERS-recommended models. *Celestial Mechanics and Dynamical Astronomy* **126**(1), 61–88 (2016)
52. Petit, G., Luzum, B.: *IERS Conventions 2010 (IERS Technical Note 36)*. Verlag des Bundesamts für Kartographie und Geodäsie, Frankfurt am Main (2010)
53. Petrov, L.: The international mass loading service. In: T. van Dam (ed.) *REFAG 2014*, pp. 79–83. Springer International Publishing, Cham (2017)
54. Petrova, N., Hanada, H.: Computer simulating of stellar tracks for observations with the lunar polar telescope. *Planetary and Space Science* **68**(1), 86–93 (2012). DOI 10.1016/j.pss.2011.10.002. *Terrestrial Planets 1*
55. Pitjeva, E.: EPM2002 and EPM2002C—two versions of high accuracy numerical planetary ephemerides constructed for TDB and TCB time scales. *Communication of IAA RAS* **155** (2003). URL <http://iaaras.ru/media/print/preprint-155.pdf>

56. Pitjeva, E.V.: Updated IAA RAS planetary ephemerides—EPM2011 and their use in scientific research. *Solar System Research* **47**(5), 386–402 (2013). DOI 10.1134/S0038094613040059
57. Pitjeva, E.V.: VLBI data are the basis for orientation of planetary ephemerides with respect to ICRF2 and improvement of other ephemeris parameters. *Transactions of IAA RAS* pp. 10–15 (2017). URL <http://iaaras.ru/en/library/paper/1673>
58. Pitjeva, E.V., Pavlov, D.A.: EPM2017 and EPM2017H. Tech. rep., Institute of Applied Astronomy RAS (2017). URL <http://iaaras.ru/en/dept/ephemeris/epm/2017>
59. Pitjeva, E.V., Pitjev, N.P.: Development of planetary ephemerides EPM and their applications. *Celestial Mechanics and Dynamical Astronomy* **119**(3), 237–256 (2014). DOI 10.1007/s10569-014-9569-0
60. Pitjeva, E.V., Pitjev, N.P.: Mass of the Kuiper belt. *Celestial Mechanics and Dynamical Astronomy* **130**(9), 57 (2018). DOI 10.1007/s10569-018-9853-5. URL <https://doi.org/10.1007/s10569-018-9853-5>
61. Preston, A., Thorpe, J.I., Miner, L.: Quasi-monolithic structures for spaceflight using hydroxide-catalysis bonding. In: 2012 IEEE Aerospace Conference, pp. 1–8 (2012). DOI 10.1109/AERO.2012.6187157
62. Ratcliff, J.T., Gross, R.S.: Combinations of Earth Orientation Measurements: SPACE2017, COMB2017, and POLE2017. JPL Publication 18-5, NASA (2018). URL <https://keof.jpl.nasa.gov/combinations/latest/SpaceCombPole2017.pdf>
63. Samain, E., Mangin, J., Veillet, C., Torre, J.M., Fridelance, P., Chabaudie, J., Féraudy, D., Glentzlin, M., Pham Van, J., Furia, M., Journet, A., Vigouroux, G.: Millimetric lunar laser ranging at OCA (Observatoire de la Côte d’Azur). *Astron. Astrophys. Suppl. Ser.* **130**, 235–244 (1998)
64. Shelus, P.J.: MLRS: a lunar/artificial satellite laser ranging facility at the McDonald Observatory. *IEEE Trans. on Geosci. and Rem. Sens.* **GE-234**, 385–390 (1985)
65. Standish, E.M.J.: JPL planetary and lunar ephemerides, DE405/LE405. Interoffice memo.312.f-98-048, NASA JPL (1998). URL <ftp://ssd.jpl.nasa.gov/pub/eph/planets/ioms/de405.iom.pdf>
66. Standish, E.M.J., Newhall, X.X., Williams, J.G., Folkner, W.M.: JPL planetary and lunar ephemerides, DE403/LE403. Interoffice memo 314.10-127, NASA JPL (1995). URL <ftp://ssd.jpl.nasa.gov/pub/eph/planets/ioms/de403.iom.pdf>
67. Turyshv, S.G., Williams, J.G., Folkner, W.M., Gutt, G.M., Baran, R.T., Hein, R.C., Somawardhana, R.P., Lipa, J.A., Wang, S.: Corner-cube retro-reflector instrument for advanced lunar laser ranging. *Experimental Astronomy* **36**(1), 105–135 (2013). DOI 10.1007/s10686-012-9324-z
68. Vasiliev, V.P., Sadovnikov, M.A., Sokolov, A.L., Shargorodski, V.D.: New ideas in retroreflector array development. In: 19h International Workshop on Laser Ranging (2014). URL <https://cdsis.nasa.gov/lw19/docs/2014/Abstracts/3024.pdf>
69. Viswanathan, V., Fienga, A., Gastineau, M., Laskar, J.: INPOP17a planetary ephemerides. *Notes Scientifiques et Techniques de l’Institut de Mécanique Céleste* **108** (2017). DOI 10.13140/RG.2.2.24384.43521
70. Viswanathan, V., Fienga, A., Minazzoli, O., Bernus, L., Laskar, J., Gastineau, M.: The new lunar ephemeris INPOP17a and its application to fundamental physics. *Monthly Notices of the Royal Astronomical Society* **476**(2), 1877–1888 (2018). DOI 10.1093/mnras/sty096
71. Wallace, P.T., Capitaine, N.: Precession-nutation procedures consistent with IAU 2006 resolutions. *A&A* **459**(3), 981–985 (2006). DOI 10.1051/0004-6361:20065897
72. Williams, J.: personal communication (2019)
73. Williams, J., Newhall, X., Dickey, J.O.: Determination of precession and nutation from lunar laser ranging analysis. *Highlights of Astronomy* **10**, 214217 (1995). DOI 10.1017/S1539299600011047
74. Williams, J.G.: Insight-building models for lunar range and range rate. *Celestial Mechanics and Dynamical Astronomy* **130**(10), 63 (2018). DOI 10.1007/s10569-018-9857-1
75. Williams, J.G., Boggs, D.H.: Tides on the Moon: Theory and determination of dissipation. *Journal of Geophysical Research: Planets* **120**(4), 689–724 (2015). DOI 10.1002/2014JE004755

76. Williams, J.G., Boggs, D.H.: Secular tidal changes in lunar orbit and Earth rotation. *Celestial Mechanics and Dynamical Astronomy* **126**(1), 89–129 (2016). DOI 10.1007/s10569-016-9702-3
77. Williams, J.G., Boggs, D.H., Folkner, W.M.: DE430 Lunar Orbit, Physical Librations, and Surface Coordinates. Jet Propulsion Laboratory Interoffice Memorandum 335-JW,DB,WF-20130722-016, California Institute of Technology (2013). URL [https://naif.jpl.nasa.gov/pub/naif/generic\\_kernels/spk/planets/de430\\_moon\\_coord.pdf](https://naif.jpl.nasa.gov/pub/naif/generic_kernels/spk/planets/de430_moon_coord.pdf)
78. Williams, J.G., Turyshv, S.G., Boggs, D.H.: Lunar laser ranging tests of the equivalence principle. *Classical and Quantum Gravity* **29**(18), 184004 (2012). DOI 10.1088/0264-9381/29/18/184004
79. Williams, J.G., Turyshv, S.G., Boggs, D.H.: The past and present Earth-Moon system: the speed of light stays steady as tides evolve. *Planetary Science* **3**(1), 2 (2014). DOI 10.1186/s13535-014-0002-5
80. Yagudina, E.I., Pavlov, D.A., Tryapitsyn, V.N., Rummyantsev, V.V.: Processing and analysis of lunar laser ranging observations in crimea in 1974-1984. In: Proceedings of the 2016 International Workshop on Laser Ranging, Potsdam, Germany (2018). URL [https://cddis.nasa.gov/lw21/docs/2018/papers/B30\\_Ignatenko\\_paper.pdf](https://cddis.nasa.gov/lw21/docs/2018/papers/B30_Ignatenko_paper.pdf)
81. Yoder, C.F., Standish, E.M.: Martian precession and rotation from Viking lander range data. *Journal of Geophysical Research: Planets* **102**(E2), 4065–4080 (1997). DOI 10.1029/96JE03642
82. Zerhouni, W., Capitaine, N.: Celestial pole offsets from lunar laser ranging and comparison with VLBI. *A&A* **507**(3), 1687–1695 (2009). DOI 10.1051/0004-6361/200912644